Mechano-regulation of tissue differentiation in osteochondral defects

D.J. Kelly & P.J. Prendergast
Centre for Bioengineering, Department of Mechanical Engineering, Trinity College, Dublin, Ireland.

Keywords: Mesenchymal stem cell; Osteochondral defect; Mechanobiology; Tissue differentiation; Apoptosis

Word count: 3629

Address correspondence to:
Prof. Patrick J Prendergast
Centre for Bioengineering
Department of Mechanical Engineering
Parsons Building
Trinity College
Dublin 2
Ireland

Tel: +353.1.6081383

Fax: +353.1.6795554

Email: pprender@tcd.ie

Submitted to: Journal of Biomechanics

First submitted: May 2003

Revised submission: January 2004

Abstract

Cartilage defects that penetrate the subchondral bone can undergo spontaneous repair through the formation of a fibrous or cartilaginous tissue mediated primarily by mesenchymal stem cells from the bone marrow. This tissue is biomechanically inferior to normal articular cartilage, and is often observed to degrade over time. The factors that control the type and quality of the repair tissue, and its subsequent degradation, have yet to be elucidated. In this paper, we hypothesise a relationship between the mechanical environment of mesenchymal stem cells and their subsequent dispersal, proliferation, differentiation and death. The mechano-regulation stimulus is hypothesised to be a function of strain and fluid flow; these quantities are calculated using a finite element model of the tissue. A finite element model of an osteochondral defect in the knee was created, and used to simulate the spontaneous repair process. The model predicts bone formation through both endochondral and direct intramembranous ossification in the base of the defect, cartilage formation in the centre of the defect and fibrous tissue formation superficially. Greater amounts of fibrous tissue formation are predicted as the size of the defect is increased. Large strains are predicted within the fibrous tissue at the articular surface, resulting in significant cell apoptosis. This result leads to the conclusion that repair tissue degradation is initiated in the fibrous tissue that forms at the articular surface. The success of the mechano-regulation model in predicting many of the cellular events that occur during osteochondral defect healing suggest that in the future it could be used as a tool for optimizing scaffolds for tissue engineering.

1. Introduction

Articular cartilage has limited reparative abilities. Purely chondral defects do not heal, and usually progress to degeneration of the surrounding cartilage (Kim et al., 1991). Osteochondral defects – that is defects that penetrate the subchondral bone – can undergo spontaneous repair. Using a rabbit model, Shapiro et al. (1993) showed that this repair is mediated by the proliferation and differentiation of mesenchymal cells that invade the defect from the underlying bone marrow. The mesenchymal cells were seen to differentiate into fibroblasts, chondrocytes and osteoblasts, synthesising new bone tissue in the base of the defect by both endochondral and direct intramembranous ossification, and synthesising cartilage tissue in the chondral region of the defect, with a layer of fibrous tissue forming at the articular surface. However over time the repair tissue begins to degenerate, with extensive fissuring and fibrillation observed in the superficial layers (Shapiro et al., 1993). Despite the poor outcome, this natural repair response still forms the rationale behind a number of orthopaedic procedures (Hunziker, 1999).

Experimental studies have shown that several physical factors such as the size and location of the defect, or the type of loading, can influence the quality, type and durability of the repair tissue. For example, rabbit model studies by Salter et al. (1982), Shimizu et al. (1987) and Kim et al. (1991) have suggested that continuous passive motion post-operatively, followed by normal activity, results in a superior repair tissue compared to the tissue that forms under normal activity alone. In a canine model, DePalma et al. (1966) observed that cartilage formation in defects in non-weight bearing areas occurred at a slower rate, and was quantitatively inferior compared to cartilage that formed in weight-bearing areas. Shapiro et al. (1993) observed variations in the relative proportions of fibrous tissue, fibrocartilage and

hyaline cartilage found in each defect, and attributed some of this variability to the fact that defects were created in various places over the articular surface and hence subject to different mechanical stresses. Convery et al. (1972) reported complete repair in defects 3 mm in diameter in horses; however incomplete repair and degenerative changes were observed in defects greater than 9 mm in diameter nine months post-operatively. While these experiments suggest that the local mechanical environment of mesenchymal stem cells within an osteochondral defect influences cellular proliferation and differentiation, and the subsequent remodelling or degradation of the repair tissue, no clear mechanobiological explanation for osteochondral defect repair has yet been given.

Mechanobiological models have been developed that hypothesise a relationship between the mechanical environment and tissue differentiation. For example, Pauwels (1960) suggested that distortional shear stress is a specific stimulus for the development of fibrous tissue, hydrostatic compression is a specific stimulus for cartilage formation and ossification only occurs after the soft tissues have provided sufficient stability to reduce mechanical stimuli below a threshold value. Based on such ideas, mathematical models have been proposed to describe tissue differentiation during fracture healing (Carter et al., 1988; Claes and Heigele, 1999; Lacroix et al., 2002; Lacroix and Prendergast, 2002; Garcia et al., 2002). All of these models have been able to predict the general patterns of tissue differentiation observed in animal experiments and go a long way towards confirming the hypotheses of mechano-regulated tissue differentiation. The models of Lacroix et al. (2002) and Garcia et al. (2002) included the effect of mesenchymal stem cell invasion of the fracture callus during healing. Stem cell access to the regenerating region was

predicted to have a considerable effect on the healing pattern and the healing rate (Lacroix et al., 2002).

In this paper, the model of mechano-regulated stem cell differentiation by strain and fluid flow is further developed to include features not considered previously but which may be important for realistic simulation of strategies for tissue engineering of connective tissues. These include the effect of mechanical stimuli on cell mitosis and cell death, as well as the influence of the tissues present on cell dispersal rates. The resulting algorithm for the prediction of mechano-regulated tissue differentiation is tested by simulating the repair of osteochondral defects of different sizes, and comparing the results to experimental observations.

2. Methods

Mechanobiological processes are driven by the local mechanical environment of the cell. Computational techniques such as finite element modelling make it possible to calculate the mechanical stimuli within the extracellular matrix of a regenerating tissue. In this paper, an osteochondral defect within the knee is analysed with a finite element model. The mechanical stimuli that would act on cells within the defect are calculated. How they control the dispersal, proliferation, differentiation and apoptosis of mesenchymal stem cells is explained by a set of equations described below.

Development of the mechano-regulation algorithm

Once the subchondral bone is penetrated, mesenchymal stem cells invade the defect from the bone marrow. These stem cells can differentiate into cells of different phenotypes i (i.e. fibroblasts, chondrocytes and osteoblasts) that produce different connective tissues j (i.e. fibrous tissue, cartilage and bone). The dispersal of cells of a

particular phenotype *i* throughout the defect can be simulated by assuming the cell population to be described by diffusive, proliferative and apoptotic processes as follows:

$$\frac{\mathrm{d}n^{\mathrm{i}}}{\mathrm{d}t} = D^{\mathrm{i}}\nabla^2 n^{\mathrm{i}} + P^{\mathrm{i}}(S)n^{\mathrm{i}} - K^{\mathrm{i}}(S)n^{\mathrm{i}}, \qquad (1)$$

where n^{i} denotes the number of cells of a particular cell phenotype *i*, D^{i} is the diffusion coefficient for cell phenotype *i*, $P^{\mathrm{i}}(S)$ is a proliferation rate and $K^{\mathrm{i}}(S)$ is a cell death rate (either necrosis or apoptosis) for cell phenotype *i* as a function of the stimulus *S*. The diffusion coefficient for cell type *i* moving through a volume of tissue is calculated as the weighted average of the diffusion coefficients for each of the tissue types *j* present at that site in the model, i.e.

$$D^{i} = \sum_{j=1}^{n_{\mathrm{t}}} D_{\mathrm{ij}}\phi_{\mathrm{j}}, \qquad (2)$$

where D_{ij} is the diffusion coefficient for cell type *i* in tissue *j*, and n_{t} is the total number of tissue types, in this case granulation tissue, fibrous tissue, cartilage and bone. ϕ_{j} denotes the volume fraction of each tissue type *j* such that:

$$\sum_{\mathrm{j=1}}^{\mathrm{n}_t} \phi_{\mathrm{j}} = 1. \qquad (3)$$

As the cells disperse throughout the defect, their number will increase due to proliferation, or decrease due to cell death. The proliferative response of each cell phenotype might be expected to be influenced by their local environment such that the rate of change in the number of cells n^{i} of the i^{th} phenotype depends on $P^{\mathrm{i}}(S)$, the proliferation rate for cell phenotype *i* as a function of a mechanical stimulus *S*, and $K^{\mathrm{i}}(S)$, the apoptosis rate for cell phenotype *i* as a function of a mechanical stimulus *S*. A quadratic relationship will be assumed between cell proliferation/apoptosis and octahedral shear strain S_{o} such that we can write:

$$P^{i}(S)n^{i} - K^{i}(S)n^{i} = a + bS_{o} + cS_{o}^{2}. \qquad (4)$$

Equation (4) can then be expressed for each cell type *i* in matrix form as follows:

$$\frac{\mathrm{d}}{\mathrm{d}t}\begin{Bmatrix} n^{mesenchymal} \\ n^{fibroblast} \\ n^{chondrocyte} \\ n^{osteoblast} \end{Bmatrix} = \begin{bmatrix} a_{mesenchymal} & b_{mesenchymal} & c_{mesenchymal} \\ a_{fibroblast} & b_{fibroblast} & c_{fibroblast} \\ a_{chondrocyte} & b_{chondrocyte} & c_{chondrocyte} \\ a_{osteoblast} & b_{osteoblast} & c_{osteoblast} \end{bmatrix} \begin{Bmatrix} 1 \\ S_{o} \\ S_{o}^{2} \end{Bmatrix}. \qquad (5)$$

As cells disperse throughout the defect, they will differentiate into different cell phenotypes depending on a local biophysical stimulus *S*. Following Prendergast et al. (1997), the stimulus for differentiation *S* is defined as:

$$S = \frac{\gamma}{a} + \frac{v}{b}, \qquad (6)$$

where γ is the octahedral shear strain and v is the fluid velocity, a and b being empirical constants (Huiskes et al., 1997). Cells can differentiate into the following cell phenotypes and synthesise a new tissue type based on the predicted value of *S*:

$n_{\text{resorbtion}} [S < n_{\text{mature}}$	osteoblast: mature woven bone	
$n_{\text{mature}} [S < 1$	osteoblast: immature woven bone	
$1 [S < m$	chondrocyte: cartilage	
S / m	fibroblast: fibrous connective tissue	(7)

where $n_{\text{resorbtion}}$, n_{mature} and m represent boundaries of the mechano-regulation diagram for tissue differentiation. In the region $0 [S < n_{\text{resorbtion}}$ bone resorbtion occurs.

Implementation of the mechano-regulation algorithm

As a first approximation the diffusion coefficient is assumed to be the same for each cell phenotype *i* passing through a particular tissue type *j*. Therefore:

$$D_{\text{mesenchymal,j}} = D_{\text{fibroblast,j}} = D_{\text{chondrocyte,j}} = D_{\text{osteoblast,j}} \quad . \tag{8}$$

The exact relationship between biophysical stimuli and cell mitosis and apoptosis has not been widely investigated. Cell mitosis has been shown to depend on the cell type (Jones et al., 1991) and the origin of the cell within the body (Brighton et al., 1991), as well as magnitude (Jones et al., 1991), frequency and number of cycles (Kasper et al., 2002) of the applied strain. Inter-patient variation has also been observed (Fermor et al., 1998). Jones et al. (1991) compared the mitosis rates of two types of osteoblast-like cells and skin fibroblasts to different magnitudes of strain. Only under the application of large strains (10,000 μstrains) was an increase in mitosis observed in all cell types, however these large strains were seen to cause de-differentiation of the osteoblasts into a fibroblast-like cell. Cell apoptosis has also been shown to depend on mechanical loading, increasing in a dose dependent manner (Loening *et al*., 2000). As a first approximation it will be assumed that only fibroblasts will have a strain dependent relationship between proliferation and mitosis, and that the proliferation of all other cell phenotypes is independent of strain such that equation (5) can be written as:

$$\frac{\mathrm{d}}{\mathrm{d}t}\begin{Bmatrix} n^{mesenchymal} \\ n^{fibroblast} \\ n^{chondrocyte} \\ n^{osteoblast} \end{Bmatrix} = \begin{bmatrix} a_{mesenchymal} & 0 & 0 \\ a_{fibroblast} & b_{fibroblast} & c_{fibroblast} \\ a_{chondrocyte} & 0 & 0 \\ a_{osteoblast} & 0 & 0 \end{bmatrix} \begin{Bmatrix} 1 \\ S_o \\ S_o^{\,2} \end{Bmatrix}, \tag{9}$$

where $a_{\text{mesenchymal}} = a_{\text{chondrocyte}} = a_{\text{bone}} = 0.05$, $a_{\text{fibroblast}} = 0$, $b_{\text{fibroblast}} = 2.667$, $c_{\text{fibroblast}} = -17.778$.

The values of the empirical constants of equation (6), as well as the boundaries of the mechano-regulation diagram for tissue differentiation (equation (7)), are taken to be the same as those used by Lacroix and Prendergast (2002) in a simulation of fracture healing. Therefore a = 3.75 %, b = 3 μms^{-1}, $n_{\text{resorbtion}}$ = 0.01, n_{mature} = 0.53 and m = 3.

When cells differentiate they synthesise new extracellular matrix, and the material properties of the repair tissue within the defect change. The material properties of each element within the finite element model are calculated based on the volume fraction ϕ_j of each tissue type within the element and the total number of cells n_c within that element. Instantaneous change of tissue type in an element was prevented by computing the volume fraction ϕ_j of a particular tissue phenotype j as the percentage of times that particular cell phenotype was predicted to form in the previous ten iterations of the model. For example, the Young's Modulus of each element would be calculated as:

$$E = \frac{(n_c^{\max} - n_c)}{n_c^{\max}} E_{granulation} + \frac{n_c}{n_c^{\max}} \sum_{j=1}^{n_t} E_j \phi_j , \qquad (10)$$

where $n_c^{\max}$ is the maximum number of cells that can occupy any one element, and E_j is the Young's Modulus of the j^{th} tissue phenotype.

Each of these cellular events was implemented into an algorithm, a graphical summary of which is presented in Fig. 1.

Implementation in osteochondral defect repair

An axi-symmetric finite element model of the knee was created which included a meniscus, a femoral chondyle and an articular cartilage layer (Fig. 2) using Diana (TNO, Delft, The Netherlands). A full thickness defect is incorporated into the finite

element model. The cartilage layer had a thickness of 2 mm and was assumed to be uniform across the femoral chondyle. The femoral chondyle was approximated as a flattened semi-sphere of radius 20 mm, consisting of a 1 mm deep layer of cortical bone overlaying a dense cancellous bone. The tibial plateau was modelled as a rigid contact layer, the permeability of which was assumed to be the same as cartilage. The model was restrained radially along the axis of rotation, and in the axial direction as shown in Fig. 2. The pore fluid pressure is set to zero at free cartilage surfaces (Fig. 2). The meniscus and the cartilage surface cannot penetrate each other in the axial direction, however the surfaces are allowed to slide relative to each other. To investigate the influence of defect size on the repair process, models of osteochondral defects 5 mm, 7 mm and 9 mm in radius were created. All defects were 5mm deep. To assess the influence of mesh density on the predicted results, three mesh densities were used for the 5mm defect, the first consisting of 400 elements, the second consisting of 1600 elements and the third consisting of 3600 elements. Complete integration was assumed between the repair tissue and the normal tissue. An axial ramp load of 800 N was applied over 0.5 seconds. All tissues were modelled as biphasic using poroelasic theory. The material properties used for each tissue type is listed in Table 1. The meniscus is modelled as transversely isotropic with a higher stiffness in the circumferential direction (E_1, E_2 = 0.5; E_3 = 100; ν_{12} = 0.1667; ν_{12} = 0.0015).

Initially the defect is cell free and filled with granulation tissue. The dispersal of cells through the defect is determined by solving equation 1, assuming the mesenchymal cells to originate from the bone marrow (Fig. 2).

3. Results

Mesh density had only a small effect on the pattern of repair predicted within the 5 mm defect (Fig. 3a-c). Small differences can be observed between the patterns of repair predicted by the intermediate and fine mesh and the coarse mesh, suggesting that the coarse mesh may not be accurate enough for this analysis. The importance of mesh density is emphasised by plotting the magnitude of strain at the articular surface as a function of time where it is found that increasing the mesh density causes larger octahedral shear strains to be computed at the articular surface (Fig. 4). This results in higher cell apoptosis predictions in the surface layer of the repair tissue as mesenchymal stem cells differentiate into fibroblasts and undergo apoptosis in the high strain environment (Fig. 4). The predicted magnitudes of octahedral shear strain in other regions of the defect were similar for the intermediate and fine mesh density models. As a compromise between efficiency and accuracy, it was decided to use the intermediate mesh density for the simulations, knowing that the only significant difference between the intermediate and fine mesh density models may be that the prediction of octahedral shear strain is underestimated in the very superficial region of the repair tissue.

The simulations show that, initially, the defect is partially shielded from the load by the intact cartilage adjacent to the defect, and the stimulus within the defect is low. This low level of mechanical stimuli favours osteogenesis. As the repair tissue begins to stiffen, it starts to support load, and chondrogenesis is favoured within the centre of the defect. Fibrous tissue is predicted to form at the articular surface due to the high magnitudes of strain and fluid flow in this region of the repairing tissue. Specifically the sequence begins by direct intramembranous ossification in the base of the defect. After some time, increased bone formation is predicted to occur by

endochondral ossification, and regions of cartilage begin to differentiate into fibrous tissue leading to a reduction in the amount of cartilage within the defect. Fibrous or cartilaginous tissue is predicted to persist at the interface between the repair tissue and the residual tissue due to higher than average fluid flows in this region.

Although the pattern of repair predicted within the defects is seen to be not very dependent on the defect size (Fig. 5), size does influence the amounts of each tissue type predicted to form within the defect (Fig. 6). After 50 iterations, greater amounts of fibrous tissue formation (28.2% in the 9mm defect, 19.6% in the 7 mm defect, 16% in the 5mm defect) and less bone formation (46.6% in the 9mm defect, 57.7% in the 7 mm defect, 64.6% in the 5mm defect) is predicted to form with increasing defect size, indicating that the stimulus for differentiation S increases with increasing defect size. Increasing the size of the defect is not predicted to increase cell apoptosis at the articular surface (Fig. 7).

In all sized defects, cell apoptosis (death) at the articular surface did not, contrary to what might be expected, lead to a reduction in cell concentration in other regions of the defect due to migration of cells to a region of lower cell concentration. It would seem that mitosis maintains the cell population within the defect despite significant cell apoptosis at the articular surface. To investigate how a reduced proliferative ability might influence cell numbers throughout the defect, the ability of cells to proliferate was removed after 30 iterations in a second analysis of the 7mm defect, allowing only cell apoptosis. After 30 iterations the defect is almost completely invaded by cells as in the first analysis. However as the simulation progresses, cell concentrations start to reduce in different regions of the defect due to migration of cells towards the articular surface (Fig. 8).

4. Discussion

The computational model presented here is a development of the model first reported by Lacroix and Prendergast (2002). Although several improvements have been made to the model, it still suffers from some of the simplifications and assumptions of the earlier work. For instance, it is still assumed that the migration of cells into the defect can be described by a diffusion equation, whereas cells may also be convected along in the fluid. While the diffusion coefficient does depend on the tissue type, it is assumed to be independent on the cell type (equation 8) in this paper. The values used for the diffusion coefficients for each tissue type were estimates, as no relevant experimental data could be found in the literature. In reality the diffusion coefficient may also be different for each cell type, which would influence the rate of repair. The theoretical model presented here could account for this should the relevant experimental data become available. Furthermore the thresholds used in the mechano-regulation diagram of tissue differentiation have yet to be established experimentally. The present paper has introduced the idea of a non-linear relationship between strain on the one hand and cell proliferation and death on the other. This idea has yet to be proved experimentally, and in the future such relationships will need to be more accurately defined from in vitro experiments such as those of Jones et al. (1991). No account is made either for rate at which cells differentiate and produce matrix, nor have we attempted to model the influences of growth factors such as TGF-β and BMP's, which have been shown to be possible regulators of tissue differentiation in a mathematical model of fracture healing (Bailón-Plaza and van der Meulen, 2001). The axi-symmetric finite element model of the knee, as well as the linear poroelastic constitutive models of the tissues, are simplifications of a complex biomechanical system. The fluid boundary conditions at the cartilage surfaces are also extremely

difficult to quantify. Wu et al. (2001) argued that under biological conditions, the fluid boundary conditions on the cartilage surface may vary from free flow to completely sealed, depending on the local stress/strain state, local cartilage permeability, and contact state. It was therefore decided to model the fluid boundary conditions at the free cartilage surface as semi-permeable. Despite these simplifications, the model has proven capable of simulating a tissue differentiation processes similar to that which occurs during osteochondral defect healing. The simulations have shown how defect sizes may influence defect repair rates, and have furthermore indicated the importance of cellular events in regulating the differentiation process.

The model successfully predicts the patterns of cellular differentiation observed experimentally in osteochondral defect healing. Metsäranta et al. (1996) analysed osteonectin and collagen type I, II and III expression in order to characterise the cellular phenotypes in the repair tissue of osteochondral defects. At early time points, high levels of type I collagen and osteonectin expression, indicating bone formation, were observed in the base of the defect, while superficially undifferentiated mesenchymal cells expressed type III collagen. It was not until later time points that collagen type II expression, an indicator of chondrogenesis, was observed. This pattern of early bone formation within the base of the defect (iterations 1-10), followed by increased chondrogenesis at later time points (iterations 10-20), is predicted by the computational model (Fig. 6). This correspondence between experimental and model predictions suggests that the model is correctly capturing some features of the tissue differentiation process. The model also successfully predicts the distribution of different tissue phenotypes within the defect. Shapiro et al. (1993) observed bone formation through both endochondral and direct

intramembranous ossification in the base of the defect, cartilage formation in the centre of the defect, and fibrous tissue formation superficially. This pattern of repair is also observed in the model (Fig. 3 and Fig. 5), suggesting that the high strain and fluid flow environment at the articular surface provokes fibrous tissue formation and inhibits chondrogenesis.

As stated in the introduction, extensive degeneration has been observed in osteochondral defect repair tissue after 6 to 12 months (Shapiro et al., 1993; Shahgaldi, 1998). The present model can be used to help develop a hypothesis to explain this degradation process. Firstly, fibrous tissue rather than hyaline-like cartilage forms at the articular surface. Mechanically this fibrous tissue is inferior to hyaline-like cartilage, and therefore it is unable to protect the fibroblasts that differentiate there and cell apoptosis results. While the cells underneath this superficial region maintain their proliferative ability, they provide a reserve of cells to replenish the cells lost due to mitosis. New mesenchymal stem cells might also be expected to invade the defect from the bone marrow. However as healing progresses, new bone formation occurs in the base of the defect, blocking the path of mesenchymal cells travelling from the bone marrow into the defect. It might also be hypothesized that this new bone formation hinders the diffusion of growth factors into the defect, thus reducing the proliferative ability of the remaining cells within the defect. Cell proliferation might also be expected to decrease in regions of high cell density due to limitations in space, nutrient diffusion or resources (Murray, 1993). In such a scenario this model predicts an overall reduction in the number of stem cells within the defect, as the rate of cell apoptosis now exceeds the limited proliferative ability of the remaining cell population. This cellular sequence of a repair tissue that is initially hypercellular, followed by a reduction in cell number as time progresses,

has been observed experimentally (Shapiro et al., 1993; Mitchell and Shepard, 1976). In the early stages of healing, this large cell population may be able to remodel and repair the fibrous tissue at the articular surface. However as the surface strains increase and apoptosis proceeds, the reduced cell population is no longer able to maintain the new tissue, resulting in tissue damage at the articular surface and eventually complete degradation of the repair tissue. This sequence of events is depicted in Fig. 9.

The applications of the model do not end at simulating the natural repair of osteochondral defects. For example, the model could be used to predict how a man-made scaffold or in vitro engineered tissue would affect the repair of osteochondral defects. Based on the results presented here it could be speculated that a critical design criteria for a cell-seeded scaffold used to repair cartilage defects would be that it provides a sufficiently rigid environment to maintain a viable cell population at the articular surface, with the hope of preventing fibrous tissue formation in this region. To this aim, the scaffold should also be designed to reduce the magnitudes of fluid flow superficially. This could be achieved by reducing the permeability of the scaffold at the articulating surface. The theoretical model could also be used in different circumstances, for example in predicting tissue differentiation around orthopaedic implants or bone defect healing in the presence of an engineered tissue. New insights into mechano-biology will increase the predictive power of computational models such as that presented here, making them an invaluable tool in the future design of traditional orthopaedic and tissue engineered implants.

Acknowledgements

This work was funded by the European Union under the BITES (Contract #: QLK3-CT-1999-00559) project.

References

Bailón-Plaza, A., van der Meulen, M. C. H., 2001. A mathematical framework to study the effects of growth factor influences on fracture healing. Journal of Theoretical Biology 212, 191-209.

Brighton, C. T., Strafford, B., Gross, S. B., Leatherwood, D. F., Williams, J. L., Pollack, S, 1991. The Proliferative and Synthetic Response of Isolated Calvarial Bone Cells of Rats to Cyclic Biaxial Mechanical Strain. Journal of Bone Joint Surgery, 73-A: 320-331.

Carter, D.R., Blenman, P.R., Beaupré, G. S., 1998. Correlations between mechanical stress history and tissue differentiation in initial fracture healing. Journal of Orthopaedic Research 7, 398-407.

Claes, L.E., Heigele, C.A., 1999. Magnitudes of local stress and strain along bony surfaces predict the coarse and type of fracture healing. Journal of Biomechanics 32, 255-266.

Convery, F. R., Akeson, W. H., Keown, G. H., 1972. The repair of large osteochondral defects. Clinical Orthopaedics 82, 253-262.

DePalma, A. F., Dockson McKeever, C., Subin, D. K., 1966. Process of repair of articular cartilage demonstrated by histology and autoradiography with tritiated thymidine. Clinical Orthopaedics 48, 230-242.

Fermor, B., Gundle, R., Evans, M., Emerton, M., Pocock, A., Murray, D., 1998. Primary Human Osteoblast Proliferation and Prostaglandin E_2 Release in Response to Mechanical Strain In Vitro. Bone, 22, 6: 637-643.

Garcia, J. M., Kuiper, J. H., Doblare, M., Richardson, J. B., 2002. A numerical model to study the mechanical influences on bone fracture healing. Proceedings of the 13th Conference of European Society of Biomechanics, 394-395.

Hunziker, E. B., 1999. Articular cartilage repair: are the intrinsic biological constraints undermining this process insuperable? Osteoarthritis and Cartilage 7, 15-28.

Huiskes, R., van Driel, W. D., Prendergast, P. J., Søballe, K., 1997. A biomechanical regulatory model of peri-prosthetic tissue differentiation. Journal of Materials Science: Materials in Medicine 8, 785-788.

Jones, D. B., Nolte, H., Scholübbers, J-G., Turner, E., Veltel, D., 1991. Biochemical signal transduction of mechanical strain in osteoblast-like cells. Biomaterials, 12: 101-110.

Kasper, D., Seidl, W., Neidlinger-Wilke, C., Beck, A., Claes, L., Ignatius, A., 2002. Proliferation of human-derived osteoblast-like cells depends on the cycle number and frequency of uni-axial strain. Journal of Biomechanics, 35: 873-880.

Kim, H. K. M., Moran, M. E., Salter, R. B., 1991. The potential for regeneration of articular cartilage in defects created by chondral shaving and subchondral abrasion. Journal of Bone and Joint Surgery 73A, 1301-1315.

Lacroix, D., Prendergast, P.J., Li, G., Marsh, D., 2002. Biomechanical model of simulate tissue differentiation and bone regeneration: application to fracture healing. Medical and Biological Engineering and Computing 40, 14-21.

Lacroix, D., Prendergast, P. J., 2002. A mechano-regulation model for tissue differentiation during fracture healing: analysis of gap size and loading. Journal of Biomechanics 35: 1163-1171.

Loening, A.M., James, I.E., Levenston, M.E., 2000. Injurious Mechanical Compression of Bovine Articular Cartilage Induces Chondrocyte Apoptosis. Arch. Biochem. Biophys., 381, 2: 205-212.

Metsäranta, M., Kujala, U. M., Pelliniemi, L., Österman, H., Heikki, A., Vuorio, E., 1996. Evidence of insufficient chondrocytic differentiation during repair of full-thickness defects of articular cartilage. Matrix Biology 15, 39-47.

Mitchell, N., Shepard, N., 1976. The resurfacing of adult rabbit articular cartilage by multiple perforations through the subchondral bone. The Journal of Bone and Joint Surgery 58A, 230-233.

Murray, J. D., 1993. Mathematical Biology. New York: Springer-Verlag.

Pauwels, F., 1960. Eine neue theorie über den einfluß mechanischer reize auf die differenzierung der stützgewebe. Z Anat Entwickl. Gesch. 121, 478-515. Translated as “A new theory concerning the influence of mechanical stimuli on the differentiation of the supporting tissues.” In: Maquet, P., Furlong, R. (Eds.), Biomechanics of the Locomotor Apparatus, Springer, Berlin, 1980, pp. 375-407.

Prendergast, P.J., Huiskes, R., Søballe, K., 1997. Biophysical stimuli on cells during tissue differentiation at implant interfaces. Journal of Biomechancis 30, 539-548.

Salter, R. B., Minister, R. R., Clements, N., Bogoch, E., Bell, R. S., 1982. Continuous passive motion and the repair of full-thickness articular cartilage defects – A one-year follow-up. Ortho. Trans. 7, 266-267.

Shahgaldi, B. F., 1998. Repair of large osteochondral defects: load-bearing and structural properties of osteochondral repair tissue. The Knee 5, 111-117.

Shapiro, F., Koide, S., Glimcher, M. J., 1993. Cell origin and differentiation in the repair of full-thickness defects of articular cartilage. Journal of Bone and Joint Surgery 75A, 532-533.

Shimizu, T., Videman, T., Shimazaki, K., Mooney, V., 1987. Experimental study on the repair of full thickness articular defects: effects of varying periods of continous passive motion, cage activity, and immobilization. Journal of Orthopaedic Research 5, 187-197.

Wu, J. Z., Herzog, W., Hasler, E.M., 2002. Inadequate placement of osteochondral plugs may induce abnormal stress-strain distributions in articular cartilage - finite element simulations. Medical Engineering & Physics, 24, 85-97.

Tables

Table 1: Material Properties

	Granulation tissue	Fibrous tissue	Cartilage	Immature bone	Mature bone	Cortical bone
Young's modulus (MPa)	0.2	2	10	1000	6000	17000
Permeability ($m^4/Ns \times 10^{-14}$)	1	1	0.5	0.1	0.37	0.001
Poisson's ratio	0.167	0.167	0.167	0.3	0.3	0.3
Diffusion co-efficient (mm^2/iteration)	0.8	0.1	0.05	0.01	0.01	-

Figures

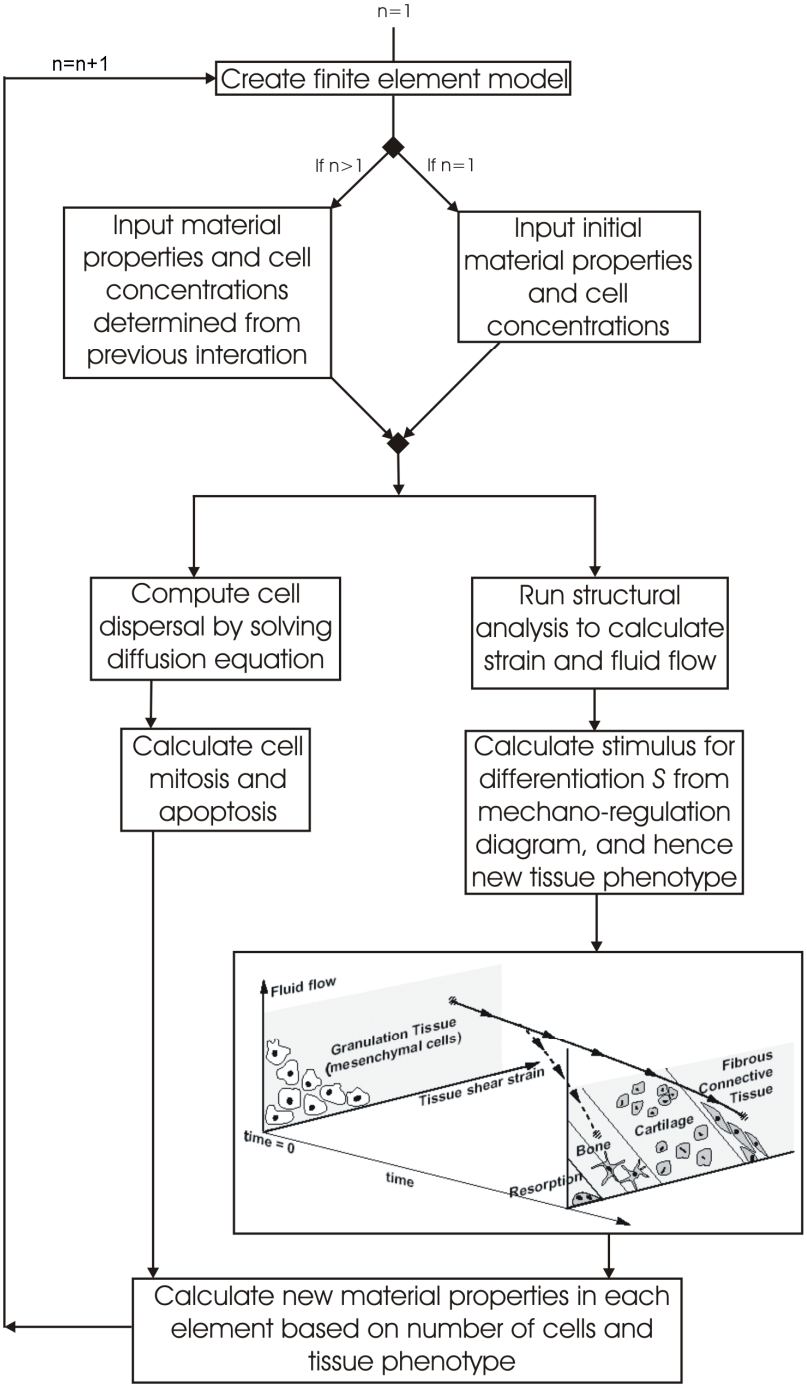

Fig. 1. Flow chart diagram of computational algorithm to model cell dispersal, proliferation, differentiation and apoptosis.

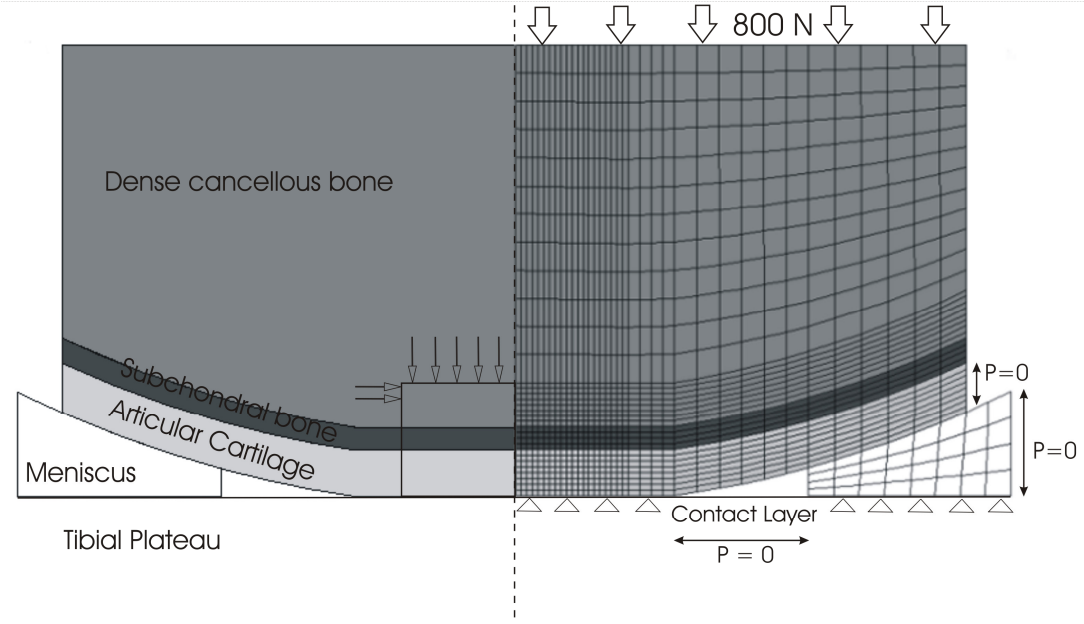

Fig. 2. Axi-symmetric finite element model of the knee with an osteochondral defect. Right: Finite element mesh illustrating loading and boundary condition. Left: 5mm defect (box) showing origin of mesenchymal stem cells (arrows).

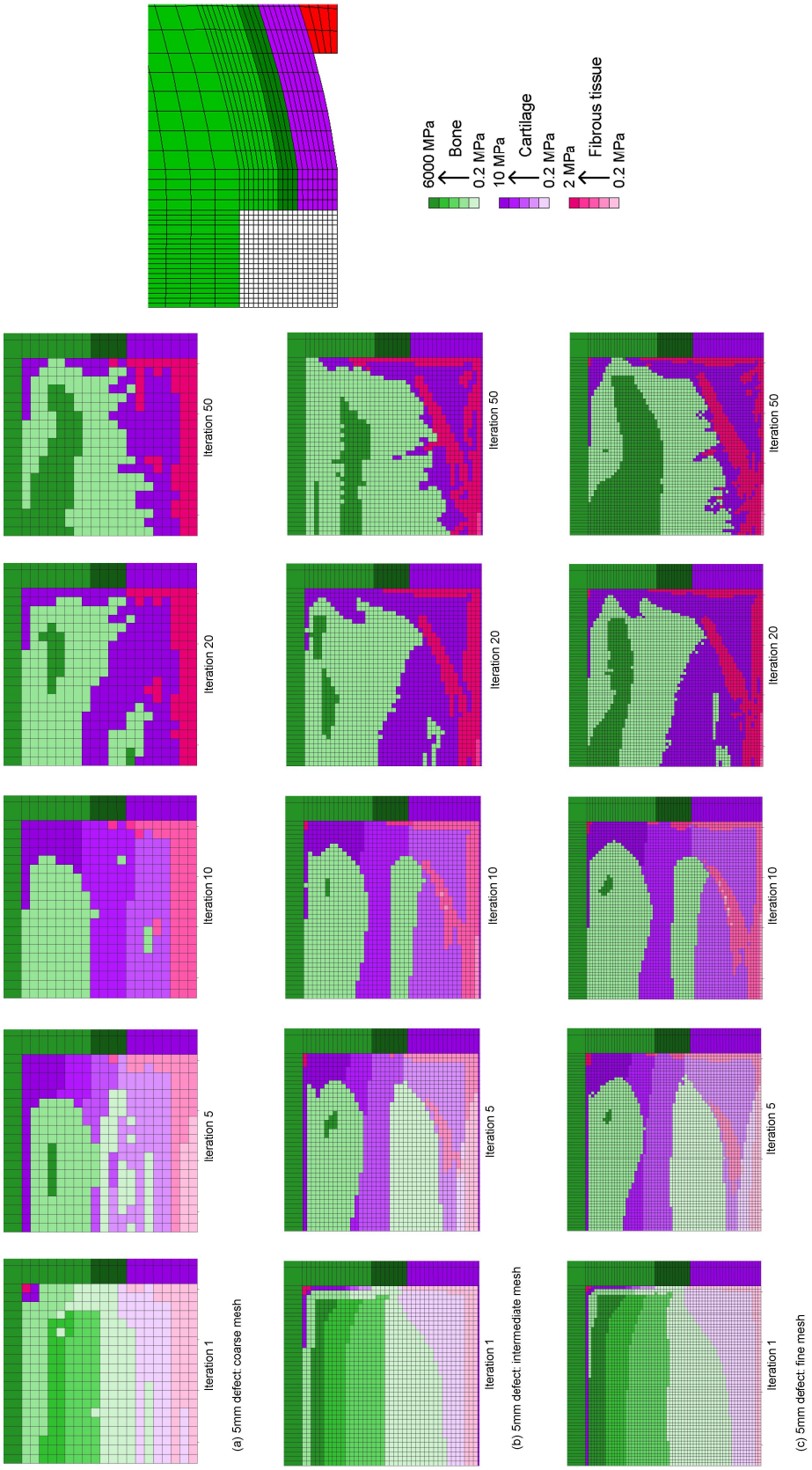

Fig. 3. Predicted patterns of tissue differentiation in 5 mm defect during simulation.

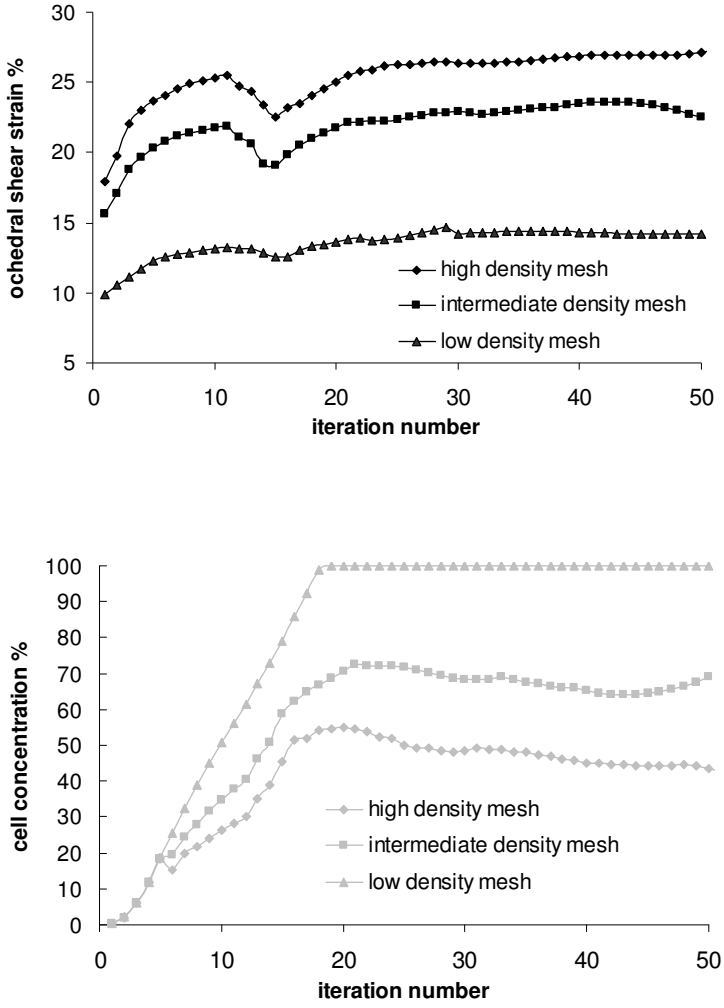

Fig. 4. Prediction of octahedral shear strain and cell concentration at the articular surface of the 5 mm defect. (Results taken from element adjacent to axis of symmetry at the articular surface, i.e. element in bottom left-hand corner of mesh illustrated in Fig. 2).

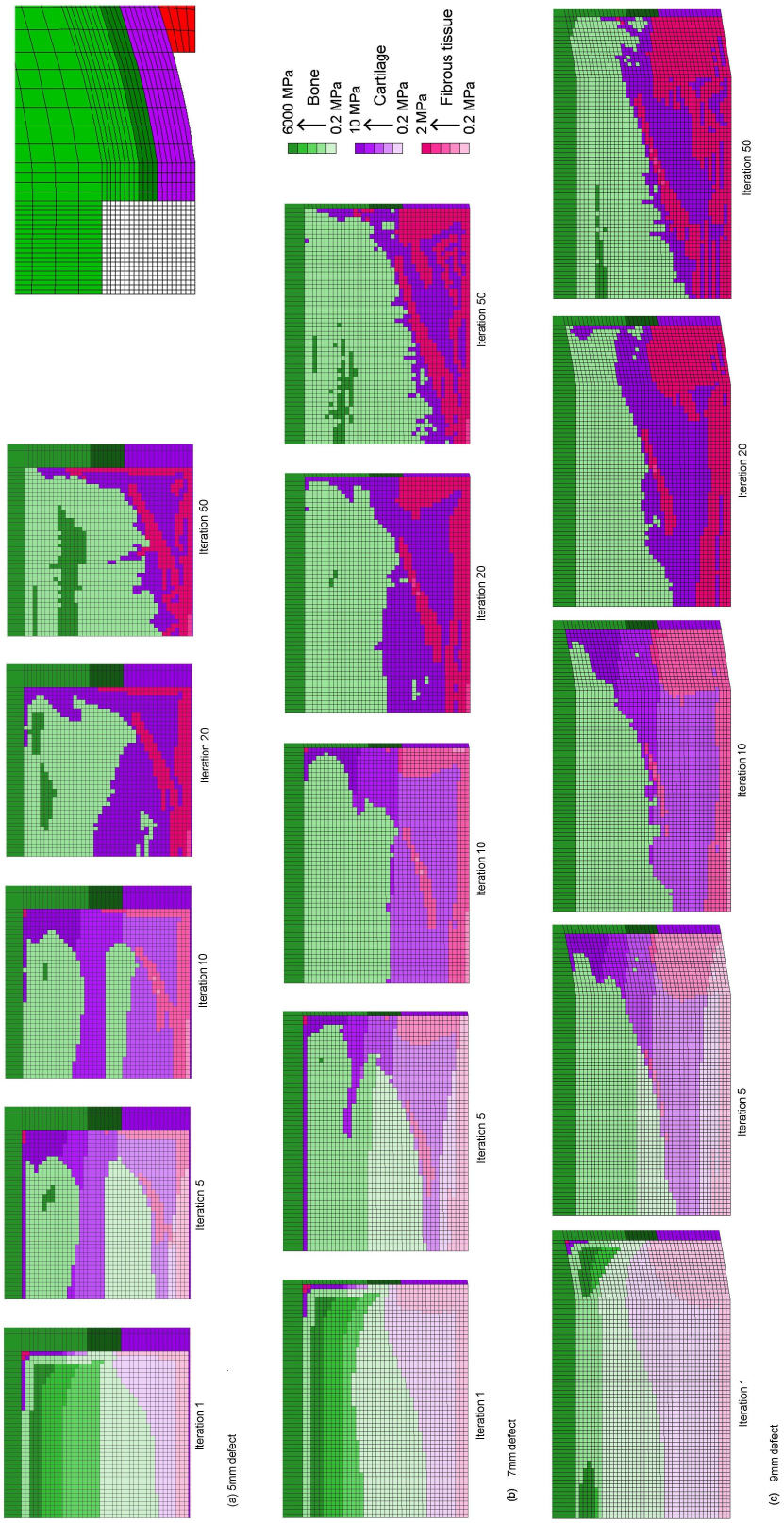

Fig. 5. Predicted patterns of tissue differentiation in 5 mm, 7 mm and 9 mm defects during simulation.

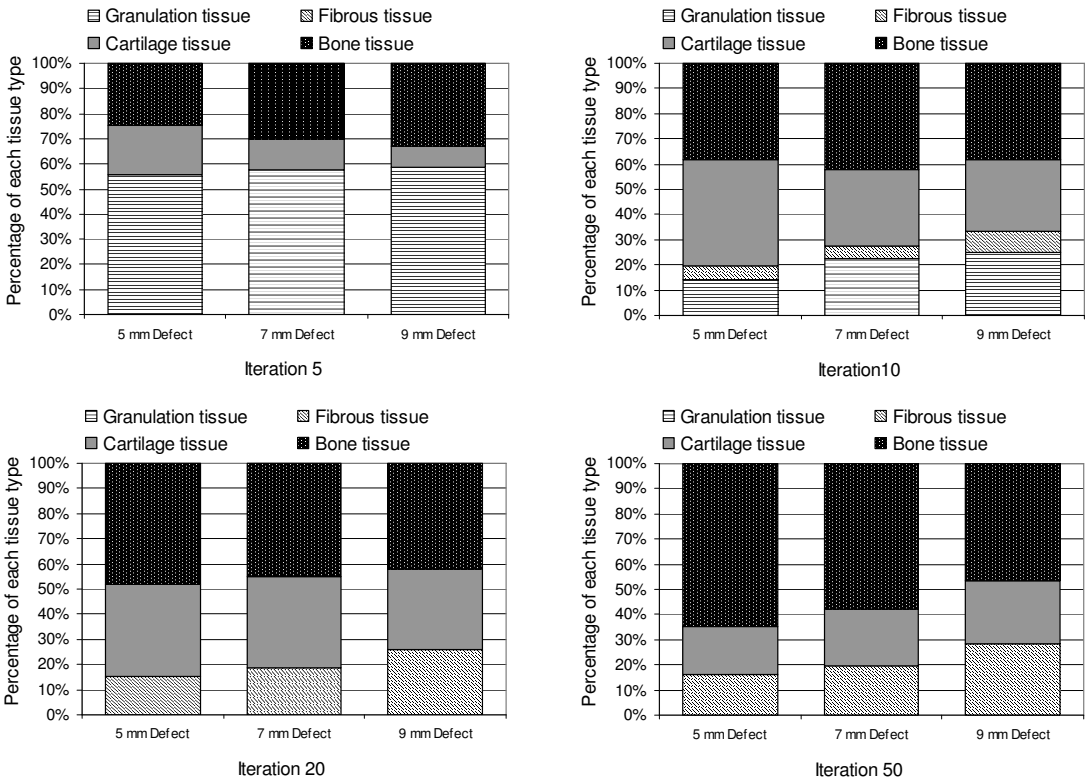

Fig. 6. Percentage breakdown of each tissue type within defect during simulation. (Note: For the purposes of this illustration granulation tissue is assumed to persist within an element until the total cell concentration exceeds 50%).

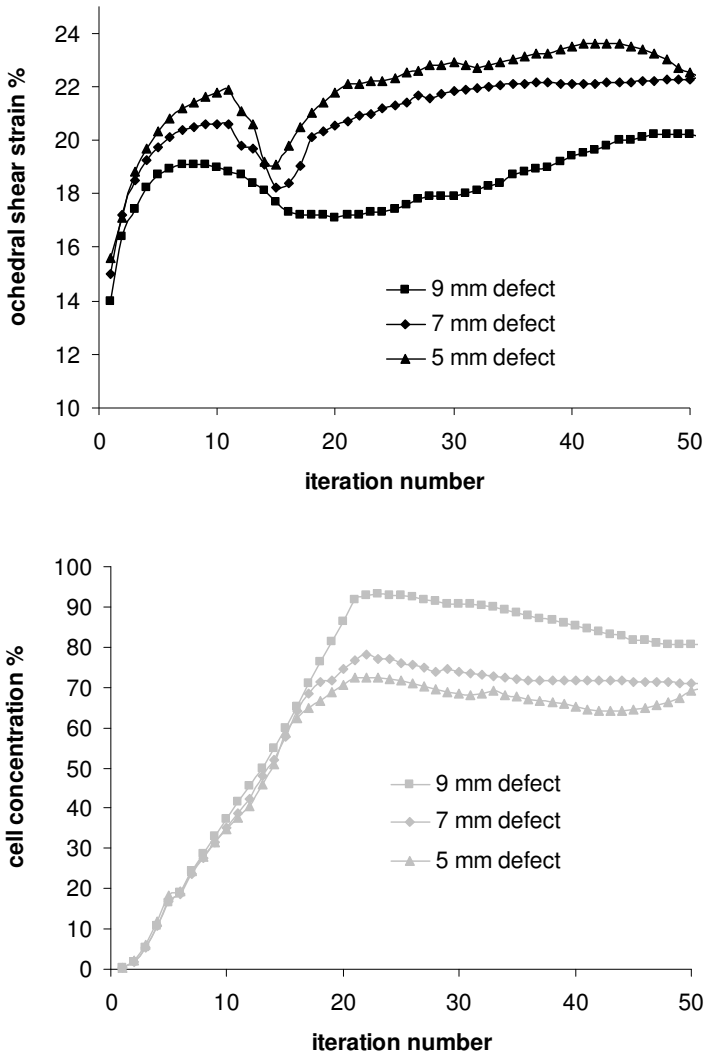

Fig. 7. Prediction of octahedral shear strain and cell concentration in the 5 mm defect, the 7 mm defect and the 9 mm defect at the articular surface.

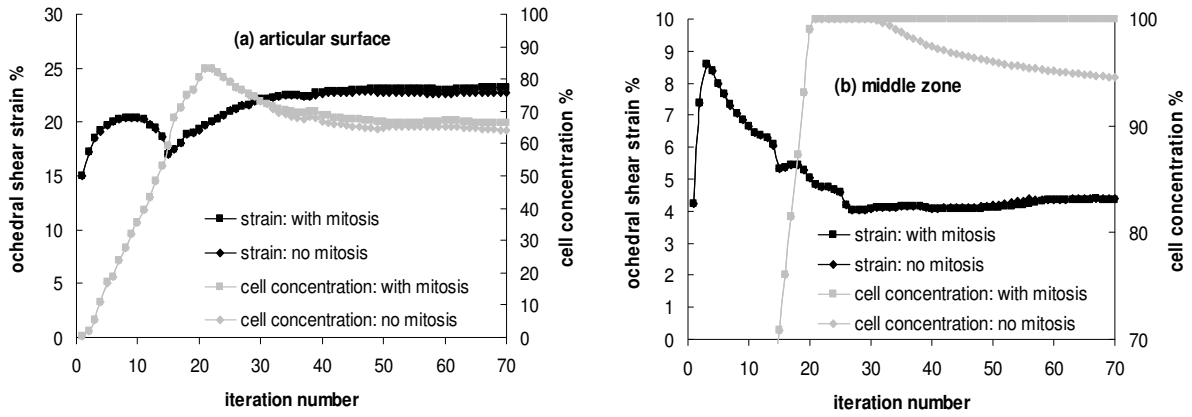

Fig. 8. Prediction of octahedral shear strain and cell concentration in the 7 mm defect with and without cell proliferation after 30 iterations at (a) the articular surface and (b) in the middle zone of the repairing tissue. (Middle zone element is taken as the element ten up from the articular surface and ten across from the axis of symmetry).

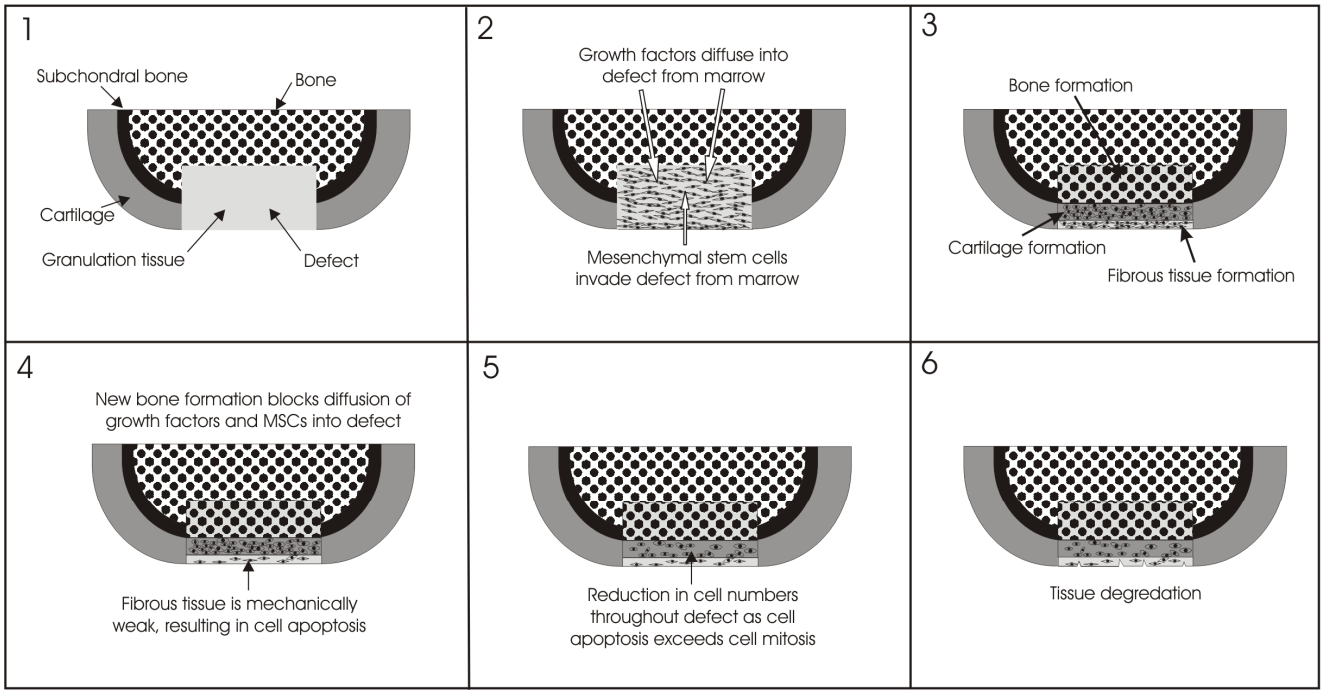

Fig. 9. Illustration of the hypothesised degradation process that occurs in osteochondral defects.